Synthesis and luminescent properties of Ln^{3+} (Eu^{3+}, Sm^{3+}, Dy^{3+})-doped lanthanum aluminum germanate $LaAlGe_2O_7$ phosphors

Yu-Chun Li [a], Yen-Hwei Chang [a,*], Yu-Feng Lin [a],
Yee-Shin Chang [b], Yi-Jing Lin [a]

[a] *Department of Materials Science and Engineering, No. 1, Ta-Hsueh Road, National Cheng Kung University, Tainan 70101, Taiwan*
[b] *Institute of Electro-Optical and Materials Science, National Formosa University Huwei, Yunlin 632, Taiwan*

Abstract

The novel phosphor of $LaAlGe_2O_7$ activated with the trivalent rare-earth Ln^{3+} (Ln = Eu, Sm, Dy) ions were synthesized by solid-state method, and their characterization and luminescent properties were investigated. The absorption, emission and excitation spectra, and decay curves were employed to study the luminescence properties. The calcined powders of the Eu^{3+}, Sm^{3+} and Dy^{3+} ions doped in the $LaAlGe_2O_7$ emit bright red, reddish orange and yellowish white light, respectively. In the photoluminescence investigations, there is a single and highly symmetric site for activator ions in the $LaAlGe_2O_7$ host lattice. The sharp emission properties show that the $LaAlGe_2O_7$ is a suitable host for rare-earth doped laser crystal and phosphor material.
© 2006 Elsevier B.V. All rights reserved.

Keywords: Luminescence; Phosphor; Rare-earth ions

1. Introduction

The energy levels of the lanthanide ions in a range of crystals were investigated and tabulated by Dieke et al. in 1968 [1], and rare-earth ions have been extensively used as the active ions in phosphors for several decades. More recently, however, the development of flat panel displays, such as field emission displays (FEDs), plasma display panels (PDPs) and thin film electro-luminescent devices (TFEL), or white light emitting diode (LED), have emerged as the principal motivation for research into rare-earth luminescence, and the present article therefore concentrates on the variety of different ways in which rare-earth luminescence has been exploited in this field [2–5]. The rare-earth ions are characterized by a partially filled 4f shell that is well shielded by $5s^2$ and $5p^6$ orbitals. The emission transitions, therefore, yield sharp lines in the optical spectra. The use of rare-earth element-based phosphor, based on "line-type" f–f transitions, can narrow to the visible, resulting in both high efficiency and a high lumen equivalent [6]. It is, therefore, urgent to find a stable, inorganic rare-earth-based phosphor with high luminescent efficiency.

The phases composed by the elements with the smaller difference of electronegativity (X), corresponds to a narrower band gap of compounds, leading to higher conductivity. The difference between the electronegativities of Si and O ($\Delta X = 1.54$) exceeds that between Ge and O ($\Delta X = 1.43$) [7]. Therefore, germanates are the host candidate in the search for phosphors with reasonable conductivity. The stoichiometric formula of germanates $MRGe_2O_7$ (where M = Al^{3+}, Ga^{3+} or Fe^{3+} and R = rare-earth ion) was reported in the early eighties to belong to the monoclinic $AlNdGe_2O_7$ structure type [8–10], space group $P2_1/c$ (no. 14). These kinds of compounds are of great interest in laser crystal physics; for instance, the incorporation of R^{3+} activators into single-centered hosts up to full substitution of all cations gives the possibility of obtaining the so-called self-activated crystals. The rare-earth cations are surrounded by nine oxygen atoms. Rare-earth ions can be separated by AlO_5 and Ge_2O_7 polyhedra in $LaAlGe_2O_7$, and the La^{3+} ion may be (totally or partially) replaced by one or more type of Ln^{3+} ions. The luminescence study of a series of such compounds provides much valuable information for optical applications. We have found the Tb^{3+} and Tm^{3+} ions in $LaAlGe_2O_7$ present intense green and

* Corresponding author. Tel.: +886 6 2757575x62941; fax: +886 6 2382800.
E-mail address: enphei@mail.ncku.edu.tw (Y.-H. Chang).

blue light emissions, respectively [11,12]. To our knowledge, no luminescence in Eu^{3+}, Sm^{3+}, Dy^{3+}-doped $LaAlGe_2O_7$ has been reported. In this paper, Eu^{3+}, Sm^{3+} and Dy^{3+} ions activated $LaAlGe_2O_7$ were prepared using a solid-state reaction, and the phases, morphologies, and photoluminescent properties were then studied.

2. Experimental

Samples of compounds of Eu^{3+}, Sm^{3+}, Dy^{3+}-doped $LaAlGe_2O_7$ were synthesized by vibrating milled solid-state reaction. The starting materials are as follows: La_2O_3, Al_2O_3, GeO_2, Eu_2O_3, Sm_2O_3 and Dy_2O_3 (purity $\geq$ 99.99%). After mechanical activation by grinding in a high energy vibro-mill for 15 min with zirconia balls in a polyethylene jar, the mixtures were calcined at 900–1300 °C for 12 h in a programmable furnace.

For determination of crystal structure, samples were investigated by X-ray diffraction (XRD). The XRD profiles were measured with a Rigaku D/max X-ray diffractometer, using Cu Kα ($\lambda = 1.5406$ Å). The ambient temperature photoluminescence (PL) spectra were obtained by Hitachi F-4500 fluorescence spectrophotometer equipped with a Xe lamp. Optical absorption spectra were measured at room temperature using Hitachi U-3010 UV–vis spectrophotometer. The standard reference used is MgO. The surface morphology was examined by high-resolution scanning electron microscopy (HR-SEM, S4200, Hitachi).

3. Results and discussion

3.1. Structure properties

The XRD profiles of the samples are shown in Fig. 1. In the diffraction pattern of the specimen heated at 1000 °C, some peaks reflecting the formation of typical $LaAlGe_2O_7$ phase was observed. However, a few peaks due to the intermediate phases

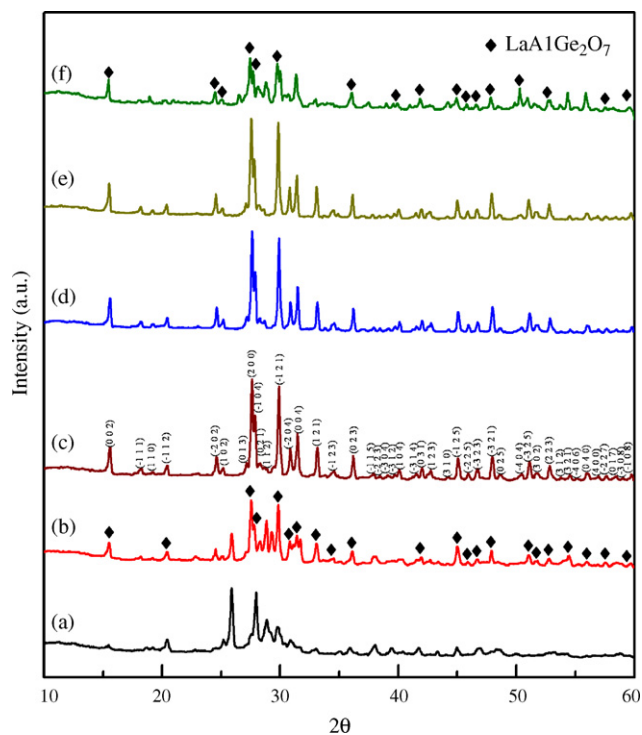
Fig. 1. The X-ray diffraction patterns of the $LaAlGe_2O_7$ powders calcined at different temperatures: (a) 900 °C, (b) 1000 °C, (c) 1100 °C, (d) 1200 °C, (e) 1250 °C, and (f) 1300 °C for 12 h.

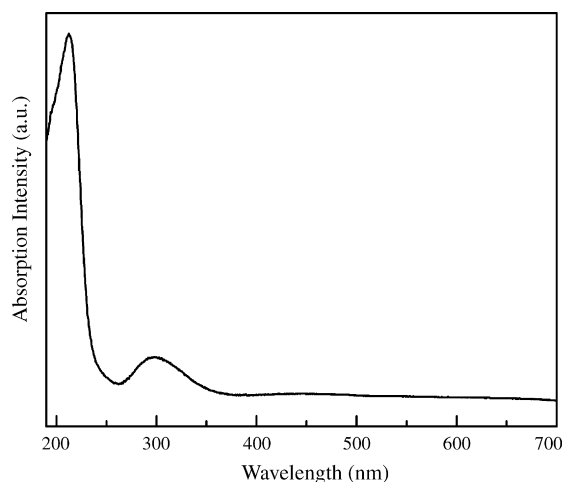Fig. 2. The UV–vis absorption spectrum of $LaAlGe_2O_7$ powder.

also appeared. Refining the positional peaks, the intermediate phases correspond to a mixture of La_2GeO_5 and La_4GeO_4. At 1100 °C, intermediate products were completely eliminated and the crystallinity of the $LaAlGe_2O_7$ powder increased with increasing calcination temperature. The SEM images show that the grain size of $LaAlGe_2O_7$ powders increased gradually as the calcination temperature increased from 1100 to 1250 °C. It appears that a higher calcination temperature enhances the atomic mobility and causes grain growth to result in better crystallinity and superior luminescence properties. However, the thermal behavior of the compound shows that the material is unstable at 1300 °C. The XRD profiles reveal that the crystallinity decreases, and several unknown impurity phases were observed at the calcination temperature of 1300 °C. The emission intensity also decreased significantly. This observation indicates that the single phase of $LaAlGe_2O_7$ was completed by heating to between 1100 and 1250 °C, and the optimum emission performance was provided by heating to 1250 °C.

The optical absorption spectrum of $LaAlGe_2O_7$ recorded in the spectral region from 190 to 700 nm at room temperature is plotted in Fig. 2. Two absorption bands for the host lattice were found in the UV region. The principal broad host absorption band was situated at 215 nm (5.77 eV), and the minor band was around 300 nm (4.13 eV). There is no obvious absorption between 350 and 700 nm. In the photoluminescence spectra, the pure $LaAlGe_2O_7$ without activators had no emission in the wavelength region measured. The $LaAlGe_2O_7$ could be classified as the extrinsic (localized) luminescence type, in which the luminescence excitation and emission processes are confined in a localized luminescence center [13].

The XRD data of the $LaAlGe_2O_7$ powders with different amounts of rare-earth ions reveals a single-phase without any impurity; all of the peaks were identified to be the monoclinic $LaAlGe_2O_7$ phase (space group $P2_1/c$). The lattice parameters of the extensive substitution of Eu^{3+} for La^{3+} in $(La_{1-x}Eu_x)AlGe_2O_7$ ($0 \leq x \leq 1$) estimated from the XRD data are shown in Fig. 3. The structure shrank gradually along the a, b and c axes as the Eu^{3+} concentration increased. It was recognized that a slight difference in the ionic radius between La^{3+}
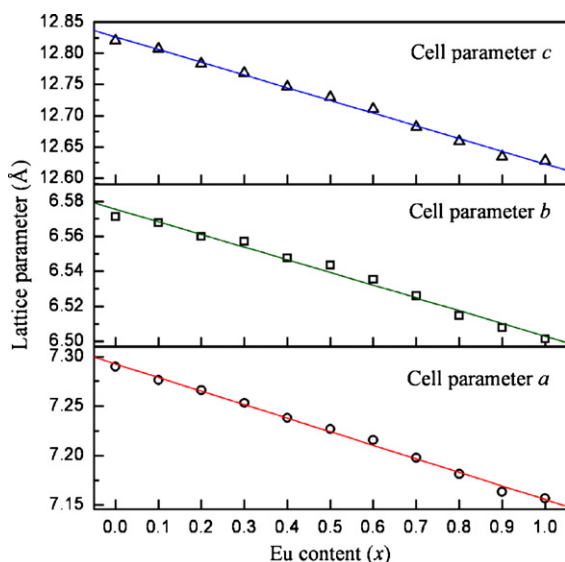
Fig. 3. The variations of the monoclinic lattice parameters a, b and c axis with the Eu^{3+} content in the $(La_{1-x}Eu_x)AlGe_2O_7$ $(0 \le x \le 1)$ (in Å).

($r_{IX} = 1.216$ Å) and Eu^{3+} ($r_{IX} = 1.120$ Å) ions resulted in a slight difference in the lattice parameter of the solid solution. A linear relationship holds between the lattice constants of the monoclinic structure and the amount of Eu^{3+} ions. The same tendency is also observed for doping with Sm^{3+} ($r_{IX} = 1.132$ Å) and Dy^{3+} ($r_{IX} = 1.083$ Å) ions. This is direct experimental evidence of the fact that the crystal can be assigned to the structural nature of the $LaAlGe_2O_7$ phase, and an indication that the rare-earth ions were satisfactorily substituted for the La^{3+} ions in the lattice. The $LaAlGe_2O_7$ powders doped with rare-earth ions at different concentrations do not significantly affect morphology. The SEM images reveal that the particles are irregularly shaped, with sizes between 1 and 6 μm.

3.2. The luminescence of Eu^{3+}-doped $LaAlGe_2O_7$

Fig. 4 presents the photoluminescence excitation, emission and absorption spectra associated with Eu^{3+} ions doped in $LaAlGe_2O_7$. The assignment of all the transitions on excitation and emission spectra are shown in the bottom right part of Fig. 4. The excitation spectrum contains two parts. A broad band near 278 nm is the charge-transfer state (CTS) band, because an electron transferred from the oxygen 2p orbital to the empty 4f orbital of europium, which may be ascribed as ligand-to-Eu^{3+} charge-transfer transitions (LMCT) [14]. The sharp peaks in the range from 280 to 550 nm are associated with typical intra-4f transitions of the Eu^{3+} ion. In comparison with the conventional Eu^{3+}-doped phosphors [15–17], it is noteworthy that the intensity of CTS transition is significantly weaker than that of intra-4f transitions. This phenomenon is uncommon, because the typical Eu^{3+}-activated phosphors always show strong CTS transition band absorption around 200–300 nm. Recently, there have been some phosphors that also show intense f–f absorption, which dominates the excitation process [18,19].

The UV–vis optical absorption spectrum of $LaAlGe_2O_7$ demonstrates that the absorption band corresponds to the UV region at 215 and 300 nm. After europium was added to $LaAlGe_2O_7$, the compounds exhibit strong broad host absorption bands and several weak absorption peaks (Fig. 4(b)). The weak absorption peaks associated with typical f–f transitions of the Eu^{3+} ion agree well with the excitation spectrum (Fig. 4(a)). However, there is no transition assigned to the host absorption in the excitation spectrum. Such a mismatch in the wavelength pattern is because the absorption spectrum is detected primarily by the numbers of occupied states in the ground level and the numbers of unoccupied states not only in the excited level but also on the transition probability, whether the transition is radiative or not. Nevertheless, only the radiative transition can be measured in the photoluminescence excitation spectrum. The absorption spectrum around 300 nm shows a complicated absorption region, in which the host absorption is mixed up with the CTS and f–f absorption of the Eu^{3+}. It might be acceptable that the CTS band overlaps with the absorption band of the host $LaAlGe_2O_7$, so that the CTS has less contribution to the excitation. Additionally, the weak CTS band may be due to the weak covalency between Eu^{3+} and O^{2-} in the $(La_{1-x}Eu_x)AlGe_2O_7$ crystallites [20]. It is recognized that no efficient energy transfer occurs between the activator and host. One of the interesting results of this work is that the excitation spectrum of the Eu^{3+}-doped $LaAlGe_2O_7$ phosphor could be strongly excited by the near-UV light, which has potential as a near-UV LED converted phosphor in solid-state lighting technology.

Most of the f–f transitions of the trivalent lanthanides are little affected by the environment. A few, however, are sensitive to the environment and become more intense. Such transitions have been called hypersensitive transitions [21]. This luminescence feature can yield structure information of a different character from that obtained by X-ray diffraction [22]. There are six obvious emission peaks between 550 and 750 nm that correspond to intra-4f-shell transitions from the excited level $^5D_0$ to lower levels ^7F_J ($J = 0–5$) for Eu^{3+} ions. Luminescence from the higher excited states, such as $^5D_1$, is not detected, indicating a very efficient nonradiative relaxation to the $^5D_0$ level [23]. The electric dipole transition $^5D_0 \rightarrow {}^7F_2$ with $\Delta J = 2$ is hypersensitive, and the intensity can vary by orders of magnitude, depending on the local environment [24]. However, the magnetic dipole transitions ($^5D_0 \rightarrow {}^7F_1$) are insensitive to the site symmetry, because they are parity-allowed. Hence, the ($^5D_0 \rightarrow {}^7F_1$)/($^5D_0 \rightarrow {}^7F_2$) emission ratio can be used as a measure of the site symmetry of Eu^{3+}. In Fig. 4(a), the strongest emission peak situated at 591 nm showing prominent and bright red light is due to the $^5D_0 \rightarrow {}^7F_1$ magnetic dipole transition, which indicates the Eu^{3+} site has inversion symmetry. In $LnAlGe_2O_7$ (Ln = rare-earth ions) crystal structure, all rare-earth ions form LnO_9 nanohedra that occupy a single crystallographic position with C_1 point symmetry [25], which is not a site symmetry center. Due to the characteristics of the space group $P2_1/c$, we can only identify the inversion center in the $LnAlGe_2O_7$ unit cell [26]. Hence, this may be the reason why the luminescence spectra have the inversion symmetry emission property.

Samples with various Eu^{3+} content had a similar spectra wavelength pattern with those in Fig. 4(a). No wavelength shift
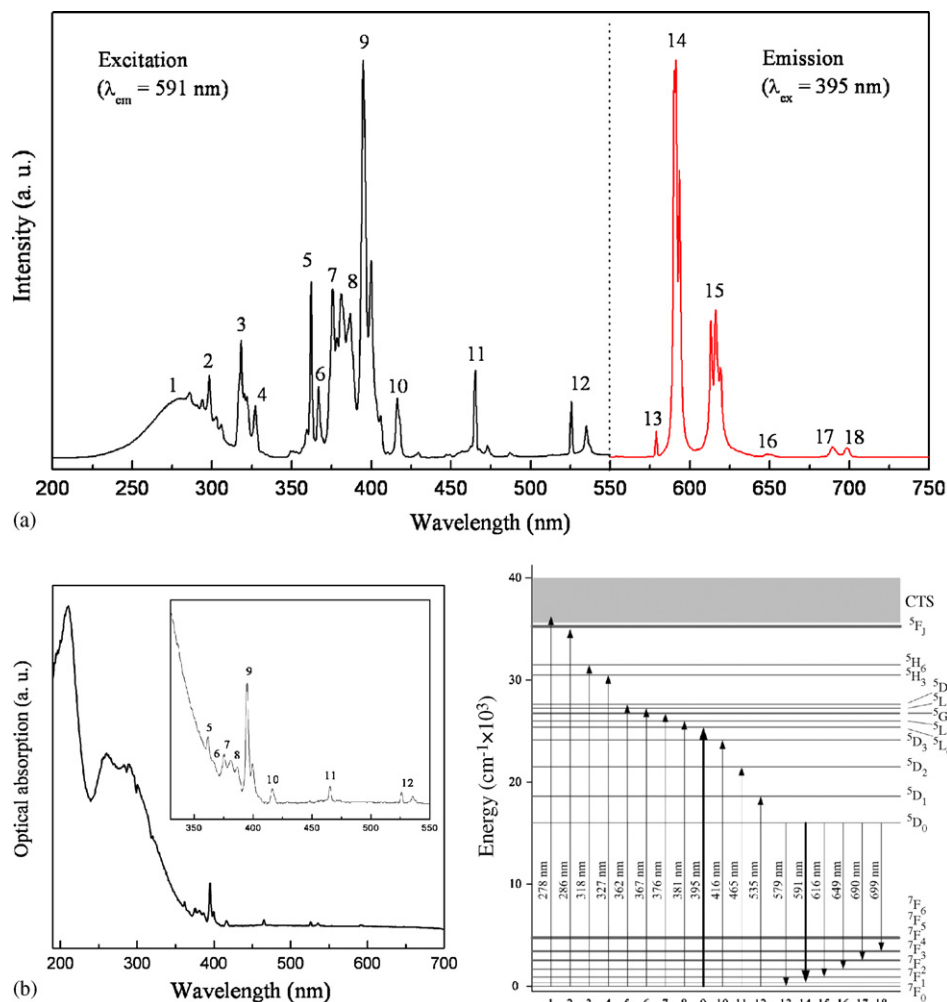
Fig. 4. Photoluminescence emission and excitation (a) and absorption spectra (b) at room temperature of LaAlGe$_2$O$_7$:Eu. The transitions depicted from 1 to 18 are shown on the bottom right.

or peak for a new site has been observed at high Eu^{3+} concentrations. The emission and decay time behaviors of the $^5D_0 \rightarrow {}^7F_1$ transition dependence of the Eu^{3+} content under excitation at 395 nm are illustrated in Fig. 5. It is well known that the lower activator doping concentrations lead to weak luminescence while higher doping concentrations cause concentration quenching. The intensity of the emission increased proportionally with Eu^{3+} concentration until saturation was reached at $x = 0.5$. Also, the lifetime declines slightly with increasing Eu^{3+} concentration to $x = 0.5$, and then begins to decrease rapidly as Eu^{3+} content increase. This phenomenon (the concentration quenching effect) is due to the rise in the number of non-radiative decay channels, as promoted by the interaction with quenching centers during the cross relaxation or energy transfer processes between excited and unexcited Eu^{3+} ions. The critical concentration was estimated to be about 50 mol%, which was much larger than the value reported for Eu^{3+}-doped phosphors, such as Y$_2$O$_3$:Eu [16] or YAG:Eu [17]. The main feature of LnAlGe$_2$O$_7$ structure is constituted by chains of the flexed LnO$_9$ nanohedra lying along the a-axis, linking alternately through an edge or a corner from the isolated AlO$_5$ distorted trigonal bipyramids in the c direction [10,25]. This structural characteristic implies that
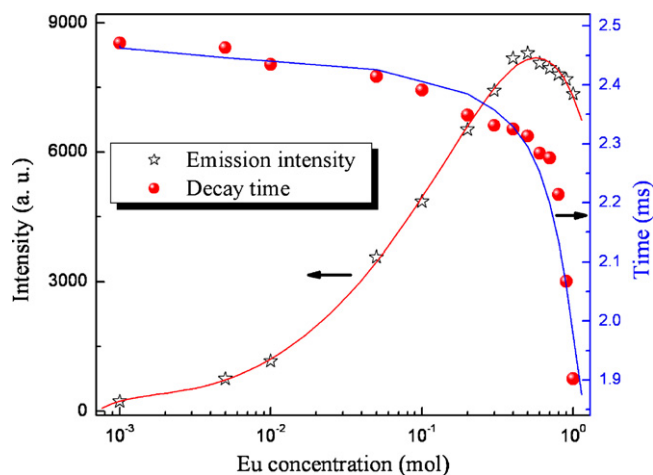

Fig. 5. The variation of emission intensity and decay time of the $^5D_0 \rightarrow {}^7F_1$ transition with Eu^{3+} concentrations in LaAlGe$_2$O$_7$ under excitation at 395 nm. The signals were detected at 591 nm.

Fig. 6. Photoluminescence emission and excitation (a) and absorption spectra (b) at room temperature of LaAlGe$_2$O$_7$:Sm. The transitions depicted from 1 to 17 are shown on the bottom right.

energy transfer between the active optical Eu^{3+} centers located in the different chains is difficult. Thus, the weak concentration quenching could be observed.

3.3. The luminescence of Sm^{3+}-doped LaAlGe$_2$O$_7$

Trivalent samarium with 4f^5 configuration has complicated energy levels and various possible transitions between f levels. The transitions between these f levels are highly selective and of sharp line spectra. The absorption, excitation and emission spectra of LaAlGe$_2$O$_7$:Sm are shown in Fig. 6. All the peaks of the excitation spectra are due to the excitation from ground-level ^{6}H$_{5/2}$ to higher energy levels of Sm^{3+} ion. The absorption spectrum shows two broad host absorption bands and several sharp peaks due to the f–f transitions of Sm^{3+}. The positions and relative intensities of excitation peaks agree well with the absorption spectrum. Generally, the typical Sm-activated phosphors usually show charge-transfer absorption of Sm^{3+}–O^{2-} interaction in the UV region. However, there was no obvious charge-transfer absorption of Sm^{3+}–O^{2-} interaction or host absorption band that could be detected in the excitation spectrum. Only direct excita-

tion of Sm^{3+} ions could be observed. It is recognized that Sm^{3+} interaction with the host lattice is very weak, and no energy transfer occurs between Sm^{3+} and host. The reddish orange light of Sm^{3+} consists of three emission peaks in the visible region near 563, 595, and 641 nm, which are assigned to the intra-4f-shell transitions from the excited level ^{4}G$_{5/2}$ to ground levels ^{6}H$_{5/2}$, ^{6}H$_{7/2}$, ^{6}H$_{9/2}$, respectively.

A series of La$_{1-x}$Sm$_x$AlGe$_2$O$_7$ samples have been synthesized with the dopant concentration ranging from 0.1 to 20 mol%. The emission and decay behaviors of the ^{4}G$_{5/2} \rightarrow \, ^6$H$_{7/2}$ transition dependence of the Sm^{3+} content under excitation at 404 nm are illustrated in Fig. 7. The emission intensity increases with Sm^{3+} concentration up to 3 mol%, and then decreases quickly. The decay time also begins to decrease rapidly at around 3 mol%. Such behaviors indicate that the concentration quenching is active.

3.4. The luminescence of Dy^{3+}-doped LaAlGe$_2$O$_7$

It is well known that the color of the trivalent dysprosium (4f^9 configuration) luminescence is close to white. The absorption,

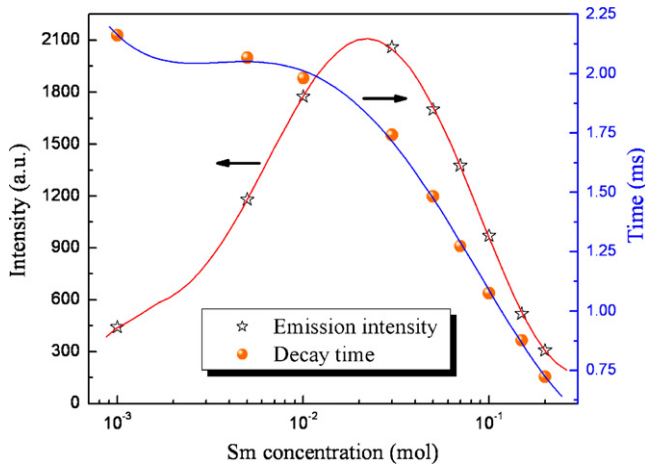Fig. 7. The relationship of emission intensity and decay time of the $^5D_0 \rightarrow {}^7F_1$ transition with Sm^{3+} concentrations in $LaAlGe_2O_7$ under excitation at 404 nm. The signals were detected at 595 nm.

excitation and emission spectra of $LaAlGe_2O_7$:Dy are shown in Fig. 8. A similar absorption spectrum as Sm^{3+} is obtained, in which the principal features are two broad bands and a number of absorption peaks in the 300–500 nm region. The broad bands correspond to host absorption while the peaks are induced by the f–f transitions of Dy^{3+}. The locations and relative intensities of the absorption peaks agree well with the excitation spectrum. In the same way, the host or Dy^{3+}–O^{2-} charge-transfer-sensitised luminescence was not observed in the short wavelength range. This phenomenon also confirms that the Dy^{3+} interactions with host lattice are weak, and no energy transfer occurs between Dy^{3+} and the host.

The strongest excitation is induced by the $^6H_{15/2} \rightarrow {}^4M_{15/2}$, $^6P_{7/2}$ transition at 351 nm. The yellowish white light is composed of blue (484 nm) and yellow (572 nm) regions. They correspond to the emission from the $^4F_{9/2}$ excited state to the $^6H_{15/2}$ and $^6H_{13/2}$ ground states, respectively. Additionally, a weaker peak is observed at 455 nm, which can be assigned to the $^4F_{7/2} \rightarrow {}^6H_{13/2}$ transition. The $^4F_{9/2} \rightarrow {}^6H_{13/2}$ transition belongs the hypersensitive transition with $\Delta J = 2$, which is strongly influenced by the outside environment of Dy^{3+}. The Dy^{3+} site
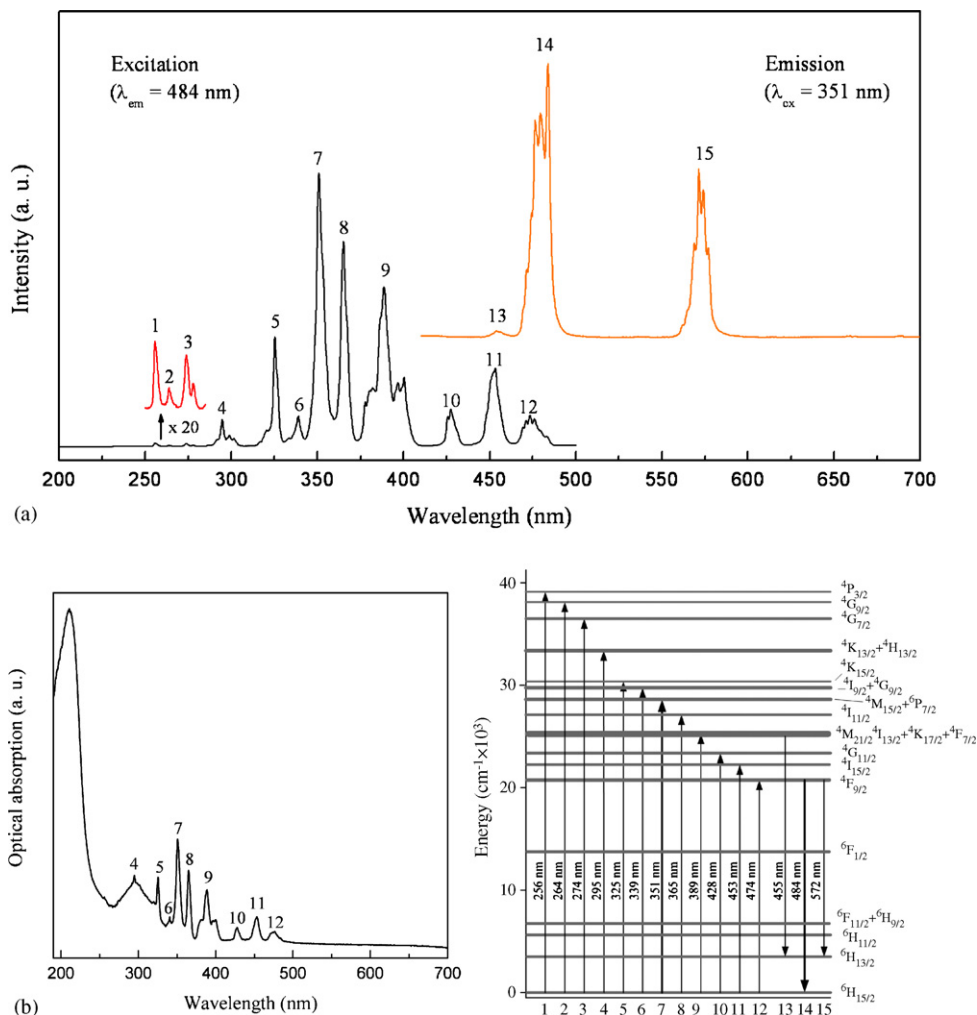

Fig. 8. Photoluminescence emission and excitation (a) and absorption spectra (b) at room temperature of $LaAlGe_2O_7$: Dy. The transitions depicted from 1 to 15 are shown on the bottom right.
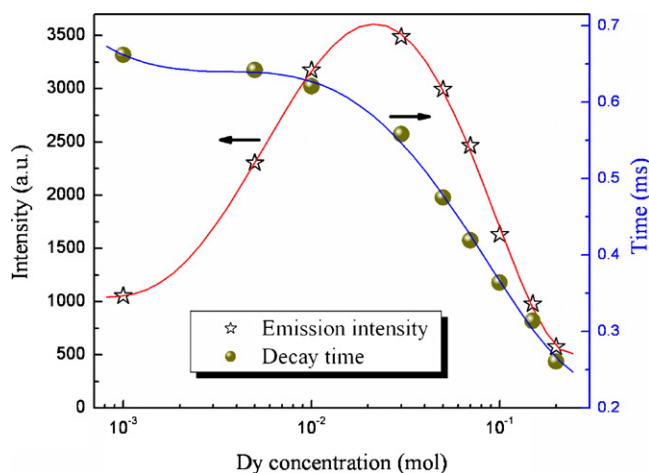
Fig. 9. The dependence of emission intensity and decay time of the $^4F_{9/2} \to {}^6H_{15/2}$ transition on Dy^{3+} concentrations in $LaAlGe_2O_7$ under excitation at 351 nm. The signals were detected at 484 nm.

must be highly symmetric because the emission intensity of $^4F_{9/2} \to {}^6H_{13/2}$ transition is less than that of $^4F_{9/2} \to {}^6H_{15/2}$ transition. The $({}^5D_0 \to {}^7F_1)/({}^5D_0 \to {}^7F_2)$ emission ratio of Eu^{3+} and $({}^4F_{9/2} \to {}^6H_{15/2})/({}^4F_{9/2} \to {}^6H_{13/2})$ emission ratio of Dy^{3+} exhibit the same trends, with variations in $LaAlGe_2O_7$. This result proves that the local symmetry of the activator ions belongs to inversion symmetry in the $LaAlGe_2O_7$ host lattice.

The relative emission intensity and decay time with varied Dy^{3+} content are represented in Fig. 9. The Dy^{3+} concentration dependence of emission intensity and decay time is analogous to Sm^{3+}. The most efficient PL intensities occur at Dy^{3+} content $x = 0.03$ for the system $(La_{1-x}Dy_x)AlGe_2O_7$. Clear concentration quenching will be observed when Dy^{3+} is above 3 mol%. It shows that the concentration quenching effect of Sm^{3+} and Dy^{3+} occurs in narrower saturation ranges than with Eu^{3+}. The cross-relaxation over ion–ion interaction between two neighbouring rare-earth ions would be beneficial to clarify this issue [27,28].

3.5. Fluorescence decay spectra

The effect of Eu^{3+} content on the $^5D_0 \to {}^7F_1$ transition decay curves is shown in Fig. 10(a). Before concentration quenching ($x < 0.5$) occurs, the decay curves show a single exponential decay and do not obviously vary with the Eu^{3+} concentration. Time-resolved $^5D_0 \to {}^7F_1$ transition shows a single exponential decay even when all sites are occupied by Eu^{3+} ions. The decay curves can be represented by the equation:

$$I = I_0 \exp\left(\frac{-t}{\tau}\right) \tag{1}$$

where I and I_0 are the luminescence intensities at time t and 0 and τ is the radiative decay time. All these curves can be well fitted into monoexponential decay, revealing that the presence of the Eu^{3+} environment is unique in according with the crystal structure. Additionally, no wavelength shift or peak for a new site has been observed for various concentrations or under different excitation wavelengths. This implies that only one local Eu^{3+} environment exists, because different centers will have different
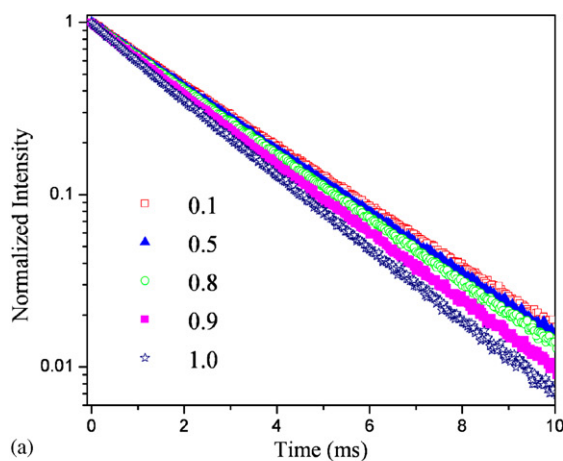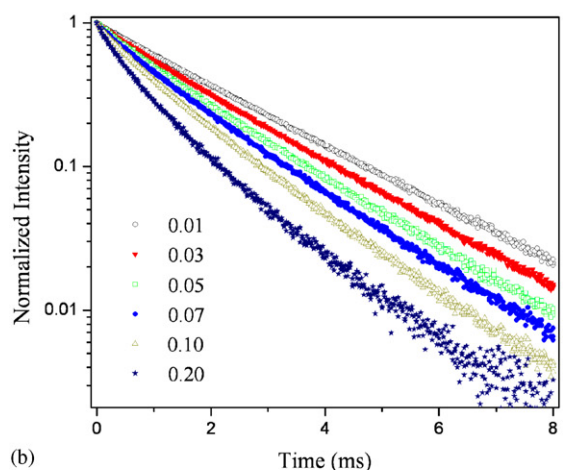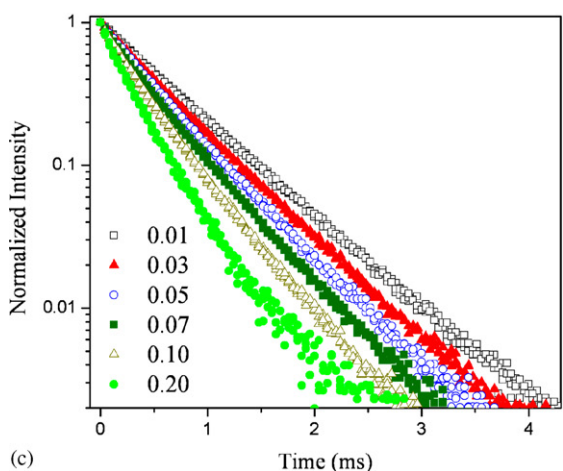
Fig. 10. Normalized decay curves of (a) $^5D_0 \to {}^7F_1$ transition for Eu^{3+}, (b) $^4G_{5/2} \to {}^6H_{7/2}$ transition for Sm^{3+}, and (c) $^4F_{9/2} \to {}^6H_{15/2}$ transition for Dy^{3+} in $(La_{1-x}Ln_x)AlGe_2O_7$ (Ln = Eu, Sm, Dy).

excitation and emission spectra. This result is inconsistent with preliminary investigations of the $LnAlGe_2O_7$-type (Ln: trivalent rare-earth ions) structure, where Ln^{3+} ions are incorporated into single-centered hosts until all rare-earth sites have been substituted [8–10,25].

Time-resolved spectra of (Sm^{3+}, Dy^{3+})-doped $LaAlGe_2O_7$ are shown in Fig. 10(b) and (c). In contrast with Eu^{3+}, the decay curves are apparently different. A single exponential

decay was observed in the diluted samples. At higher concentrations ($x > 0.03$), however, the observed decay curves were non-exponential, and the non-exponential change becomes more prominent as (Sm^{3+}, Dy^{3+}) content increases, revealing that more than one relaxation process exists. When the luminescent centers have different local environments, the associated ions will relax at different rates. If the rates are dramatically different, then diverse decay curves are likely to be observed. Nevertheless, samples with low (Sm^{3+}, Dy^{3+}) content would minimize the effects of the interactions between optically active ions. Hence, the low-doped samples yield single exponential decay curves with a long lifetime, eliminating this possibility. Additionally, it is unlikely that only one site with the shorter lifetime is populated for higher concentrations.

As mentioned before, cross-relaxation occurs easily between two neighbouring rare-earth ions. This is the process whereby excitation energy from an ion decaying from a highly excited state promotes a nearby ion from the ground state to the metastable level. In Sm^{3+}, the energy gap between the $^4G_{5/2}$ and $^6F_{9/2}$ levels is close to that between the $^6H_{5/2}$ and $^6F_{9/2}$ levels. As a result, if the Sm^{3+} concentration is sufficiently high, the higher energy level emission can be easily quenched in favor of the lower energy level emission [27]. In the case of Dy^{3+} the energy of the $^4F_{9/2} \rightarrow {}^6F_{11/2} + {}^6H_{9/2}$ transition matches the one of the $^6H_{15/2} \rightarrow {}^6F_{11/2} + {}^6H_{9/2}$ transition [28]. With the increase of Dy^{3+} concentration, the distance between Dy^{3+} ions decreases; subsequently, the energy transfer between Dy^{3+} ions becomes more frequent. Therefore, the energy transfer process between the activator ions (Sm^{3+} and Dy^{3+}) provides an extra decay channel to change the decay curves, resulting in a nonexponential decay curve.

In many cases, the concentration quenching is due to energy transfer from one activator to another until an energy sink in the lattice is reached, which is related to the interaction between an activator and another ion. For this reason, it is possible to obtain the critical distance (R_c) from the concentration quenching data. R_c is the critical separation between donor (activator) and acceptor (quenching site), for which the nonradiative transfer rate equals the internal decay rate. Blasse [29] assumed that for the critical concentration the average shortest distance between nearest activator ions is equal to the critical distance. The $LaAlGe_2O_7$ contains a unique crystallographic site available for the activator (substitute for La^{3+}), so that only one type of centre is present. Hence, we can obtain the critical distance from the concentration quenching data using the following equation:

$$R_c = 2\left(\frac{3V}{4\pi x_c N}\right)^{1/3} \tag{2}$$

where x_c is the critical concentration, N the number of La^{3+} ions in the $LaAlGe_2O_7$ unit cell (activator ions are assumed to be introduced solely into La^{3+} sites), and V is the volume of the unit cell (545.45×10^{-30} m^3 in this case). The critical concentration was estimated to be about 50 mol% for Eu^{3+} and 3 mol% for Sm^{3+} and Dy^{3+}, where the emission intensity and decay time measured begin to decrease quickly. Using the above equation,

the R_c was determined to be about 8.05 Å for Eu^{3+} and 20.55 Å for Sm^{3+} and Dy^{3+}.

4. Conclusions

A novel phosphor, Eu^{3+}, Sm^{3+}, Dy^{3+}-doped $LaAlGe_2O_7$, were synthesized and its luminescence properties have been investigated. The XRD profiles show that the lattice parameters of the compounds ($La_{1-x}Ln_x)AlGe_2O_7$ ($x = 0$–1) exhibit a linear relationship, indicating that Ln^{3+} ions are well substituted for La^{3+} ions to form stable solid solutions. In (Eu^{3+}, Sm^{3+}, Dy^{3+})-doped $LaAlGe_2O_7$, the absorption spectra are different from the excitation spectra near room temperature, suggesting that there are two kinds of absorption bands: one results in luminescence but the other does not. The hypersensitive transitions of $^5D_0 \rightarrow {}^7F_2$ (Eu^{3+}) and $^4F_{9/2} \rightarrow {}^6H_{13/2}$ (Dy^{3+}) are relatively lower than those of the insensitive transitions in $LaAlGe_2O_7$. This is conceivable that the $LaAlGe_2O_7$ structure provides high inversion symmetry sites for activator (Eu^{3+}, Dy^{3+}) ions. Lifetime measurements confirm the presence of a single activator environment in $LaAlGe_2O_7$. The emission peaks of all the samples are very sharp, with the full-width at half maximum in the range of 4–9 nm, making them attractive candidates for use in optical applications.

Acknowledgement

References

[1] G.H. Dieke, H.M. Crosswhite, H. Crosswhite, Spectra and Energy levels of Rare-Earth Ions in Crystals, Wiley, New York, 1968.
[2] C. Duan, J. Yuan, X. Yang, J. Zhao, Y. Fu, G. Zhang, Z. Qi, Z. Shi, J. Phys. D: Appl. Phys. 38 (2005) 3576.
[3] A. Komeno, K. Uematsu, K. Toda, M. Sato, J. Alloys Compd. 408–412 (2006) 871.
[4] A.H. Kitai, Thin Solid Films 445 (2003) 367.
[5] V. Sivakumar, U.V. Vardaraju, J. Electrochem. Soc. 152 (10) (2005) H168.
[6] C. Feldmann, T. Justel, C.R. Ronda, P.J. Schmidt, Adv. Funct. Matter 13 (7) (2003) 511.
[7] J.E. Hubeey, Inorganic Chemistry: Principles of Structure and Reactivity, 2nd ed., Harper and Row Publisher Inc., New York, 1978.
[8] O. Jarchow, K.-H. Klaska, H. Schenk, Naturwissenschaften 68 (1981) 475.
[9] O. Jarchow, K.-H. Klaska, H. Schenk-Strauss, Z. Kristallogr. 172 (1985) 159.
[10] A.A. Kaminskii, B.V. Mill, A.V. Butashin, E.L. Belokoneva, K. Kurbanov, Phys. Stat. Sol. (a) 103 (1987) 575.
[11] Y.C. Li, Y.H. Chang, Y.F. Lin, Y.S. Chang, Y.J. Lin, Electrochem. Solid-State Lett. 9 (8) (2006) H74.
[12] Y.C. Li, Y.H. Chang, Y.F. Lin, Y.J. Lin, Y.S. Chang, Appl. Phys. Lett. 89 (2006) 081110.
[13] D.R. Vij, Luminescence of Solids, Plenum Press, New York, 1998, p. 97.
[14] G. Blasse, J. Chem. Phys. 45 (7) (1966) 2356.
[15] R. Schmechel, M. Kennedy, H. von Seggern, H. Winkler, M. Kolbe, R.A. Fischer, X.M. Li, A. Benker, M. Winterer, H. Hahn, J. Appl. Phys. 89 (2001) 1679.
[16] Y. Sun, L. Qi, M. Lee, B.I. Lee, W.D. Samuels, G.J. Exarhos, J. Lumin. 109 (2004) 85.

[17] Y. Zhou, J. Lin, M. Yu, S. Wang, J. Alloys Compd. 375 (2004) 93.

[18] V. Sivakumar, U.V. Varadaraju, J. Electrochem. Soc. 150 (10) (2005) H168.

[19] S. Neeraj, N. Kijima, A.K. Cheetham, Chem. Phys. Lett. 387 (2004) 2.

[20] B.S. Tsai, Y.H. Chang, Y.C. Chen, Electrochem. Solid-State Lett. 8 (7) (2005) H55.

[21] C.K. Jørgensen, B.R. Judd, Mol. Phys. 8 (1964) 281.

[22] G. Blasse, J. Inorg. Nucl. Chem. 30 (1968) 2091.

[23] D. Ananias, M. Kostova, F.A. Almeida Paz, A. Ferreira, L.D. Carlos, J. Klinowski, J. Rocha, J. Am. Chem. Soc. 126 (2004) 10410.

[24] S. Shionoya, W.M. Yen, Phosphor Handbook, CRC Press, Boca 303 Raton, 1999, p. 190.

[25] G. Lozano, C. Cascales, C. Zaldo, P. Porcher, J. Alloys Compd. 303–304 (2000) 349.

[26] E.A. Juarez-Arellano, J. Campa-Molina, S. Ulloa-Godinez, L. Bucio, E. Orozco, Mater. Res. Soc. Symp. Proc. 848 (2005) 293.

[27] G. Blasse, G.J. Dirksen, J. Electrochem. Soc. 127 (4) (1980) 978.

[28] L. Nagli, D. Bunimovich, A. Katzir, O. Gorodetsky, V. Molev, J. Non-Cryst. Solids 217 (1997) 208.

[29] G. Blasse, Philips Res. Rep. 24 (1969) 131.